Pooled CRISPR screens identifies key regulators of bovine stem cell expansion for cultured meat

Check for updates

Amit Zirman[1,2], Mamoun Abed El-Nabi[1,3], Ella Samuel[1,4], Leon Anavy [5,6], Zohar Yakhini[5,6], Iftach Nachman [2] & Roni Rak [1] ✉

Cultured meat presents a sustainable alternative to traditional meat production but faces significant challenges in scalability and cost efficiency. A key limitation is the restricted proliferation capacity of bovine mesenchymal stem cells (bMSCs), a widely used cell source in the field. Using a pooled, lentiviral CRISPR knockout screen, we interrogated 3000 CRISPR guides targeting 600 genes involved in stem cell regulation or proliferation. Notably, knockouts of *TP53* and *PTEN* significantly increased proliferation rates and delayed senescence. Validation with individual gene knockouts confirms these effects, showing enhanced growth but reduced differentiation potential. We also identified chondrogenic differentiation as a promising target whose repression may further promote MSC expansion. These findings demonstrate the utility of CRISPR screening for optimizing bovine stem cell traits and offer a path toward more scalable cultured meat production in the future.

The global demand for meat continues to rise[1], with projections suggesting a 14% increase in production and consumption from 2020 to 2030[2,3]. However, conventional animal agriculture presents significant environmental and public health challenges[4], including intensive resource utilization (land, water, and energy), driving deforestation and biodiversity loss[5–7], substantial greenhouse gas emissions, contribution to antibiotic resistance, and potential for zoonotic disease transmission[8]. In response to these challenges, cultured meat, also known as lab-grown or cultivated meat, has emerged as a promising alternative[9,10]. This innovative approach aims to provide a sustainable and humane substitute for traditional meat production by in vitro proliferation of animal cells in a controlled environment, eliminating the need for live animals. Cultured meat relies on stem cells, which can both proliferate exponentially and differentiate into specialized, edible tissues such as muscle (myocytes) and fat (adipocytes)[11,12]. The process involves extracting stem cells, adapting them to in vitro conditions, expanding their biomass, and inducing specialization into mature tissues for final processing. While this approach offers potential solutions to the issues associated with conventional meat production[13,14], the current state of cultivated meat faces significant challenges, including high costs, scalability issues, and the need for further technological advancements[15].

This study addresses one of the key challenges in cultured meat production: developing efficient, scalable cell lines[16]. Various cell types are

utilized for this purpose, including mesenchymal stem cells (MSCs)[17], embryonic stem cells (ESCs), induced pluripotent stem cells (iPSCs), and primary muscle or adipose cells. ESCs and iPSCs offer broad differentiation potential but face challenges related to complexity, cost and differentiation efficiency. Primary differentiated cells exhibit efficient lineage commitment but are limited in proliferation capacity and scalability. MSCs offer a practical balance of multipotency, ease of culture, and industrial relevance, accounting for approximately 25% of cell sources used in the cultured meat sector[18]. They are readily isolated from adult tissues[19], and can differentiate into mesodermal lineages such as osteocytes (bones), chondrocytes (cartilage), adipocytes (fat), or myoblasts (muscle)[20], with well-established protocols for culture and differentiation[21]. However, their limited proliferation capacity remains a bottleneck for large-scale application.

MSCs face two key proliferation constraints: slow intrinsic growth rates and replicative senescence. While MSCs divide more rapidly compared to terminally differentiated primary cells, their doubling times remain substantially longer than those of pluripotent stem cells[16,22], implying underutilized molecular mechanisms could accelerate their division. A second limitation arises from progressive telomere shortening and stress accumulation[23], which drive irreversible senescence, a growth arrest state restricting large-scale expansion[24]. To address these challenges, strategies must either enhance baseline proliferation through cell-cycle manipulation

[1]Institute of Animal Science, Agricultural Research Organization—Volcani Institute, Rishon LeZion, Israel. [2]The George S. Wise Faculty of Life Sciences, Tel Aviv University, Tel Aviv, Israel. [3]The Mina and Everard Goodman Faculty of Life Sciences, Bar-Ilan University, Ramat Gan, Israel. [4]Faculty of Agriculture, Food and Environment, Hebrew University of Jerusalem, Rehovot, Israel. [5]School of Computer Science, Reichman University, Herzliya, Israel. [6]Faculty of Computer Science, Technion, Haifa, Israel. ✉e-mail: ronir@volcani.agri.gov.il

or delay senescence by mitigating aging mechanisms. Targeted genetic editing of these dual processes could optimize MSC expansion efficiency while maintaining their essential multipotency and differentiation potential, ultimately advancing scalable cultured meat systems.

To optimize MSC proliferation, we employed a CRISPR knockout screening approach, which enables systematic perturbation of thousands of genes to identify those with significant physiological roles[25,26]. In pooled screens, a complex library of guide RNAs and Cas9 is delivered to a heterogeneous cell population, allowing cells with advantageous mutations to be enriched through competition. In contrast, arrayed screens test each sgRNA in separate wells, enabling precise genotype-to-phenotype mapping, but at significantly higher cost and lower throughput[23]. Another key consideration is the scope of the screen: whole-genome versus targeted. While whole-genome screens provide broad coverage across the transcriptome, they are more difficult to scale and interpret, as the majority of sgRNAs have no functional effect. We selected a pooled, targeted approach to balance scalability, cost-effectiveness, and the ability to leverage proliferation as a straightforward enrichment phenotype. By enabling cells to compete in a shared environment, this strategy efficiently uncovers genetic factors driving MSC proliferation, potentially advancing scalable cultured meat production.

Our study aims to expand the application of CRISPR screening in bovine cells, focusing specifically on enhancing proliferation in bMSC, and thus addresses one of the key challenges in cultured meat production: scalability and cost-effectiveness. This approach has the potential to significantly improve the efficiency of cultivated meat, bringing us closer to a sustainable alternative to traditional meat production that can meet the growing global demand for protein while mitigating environmental and health concerns associated with conventional livestock farming.

Results

Building a bovine-specific CRISPR screening system: MSC isolation, validation, transduction, and CRISPR activity assessment

To enhance the proliferation rate of bMSCs for cultured meat production, we performed a CRISPR knockout screen to identify key genes and pathways regulating cell proliferation (Fig. 1A). This screen required both isolated MSCs and a pooled CRISPR single-guide RNA (sgRNA) library targeting 603 genes, including transcription factors and proliferation-related genes. In this study, we specifically focus on adipose-derived bMSCs, as their enhanced adipogenic differentiation potential makes them particularly suitable for generating fat tissue, a critical component of cultured meat.

Accordingly, we first isolated and characterized adipose-derived bMSCs (AD-bMSCs) from a 3-month-old calf, following an established protocol[27]. To evaluate the proliferative capacity of the isolated bMSCs, we tracked population doubling time (PDT) over 156 days. Proliferation remained stable until day 79, with an average PDT of 37.7 ± 8.0 h. After day 79, the doubling rate progressively declined, indicating a gradual loss of proliferative capacity (Fig. 1B). To determine whether this decline was connected to senescence, we performed senescence-associated β-galactosidase (SA-β-gal) staining at early (day 20) and late (day 80) passages. A significant increase in the percentage of senescent cells was observed in late-passage compared to early passage cells (average of 35% and 11.7% respectively), while etoposide-treated control cells showed a high percentage of senescent cells (87.8%), indicating that at least some of the decline in proliferation rate can be attributed to an increase in population senescence (Fig. 1C).

We next tested the cells' stemness by verifying their differentiation potential into adipocytes and chondrocytes (Fig. 1D) and by expression of MSC surface markers CD29 and CD44 (Fig. 1E, $p < 0.001$, t-test). To assess the genetic engineering capabilities of AD-bMSCs, we evaluated their transduction using lentivirus. Two plasmids were tested: one expressing GFP and the other expressing Cas9 nuclease. Flow cytometry confirmed successful GFP transduction in both bMSCs and HEK293T cell lines, with approximately 49% of bMSCs and 80% of HEK293T cells showing significantly higher green fluorescence compared to untransduced populations

($p = 0.004$ and $p < 0.001$, respectively, t-test, Fig. 1F). Related data, including gating strategy, senescence imaging, additional adipogenesis analysis, and transduction optimization are shown in Fig. S1. Cas9 expression was verified by reverse transcription PCR of RNA from Cas9-transduced cells (Fig. 1G). With successful transduction and Cas9 expression confirmed, we proceeded to construct a targeted sgRNA library to identify genes involved in MSC proliferation.

CRISPR short-term proliferation screen enriches and depletes known and novel genes

We designed a focused bovine-specific CRISPR knockout library to enhance MSC proliferation by targeting 603 Bos taurus genes related to proliferation (Fig. 2A). The library included transcription factors[28] and genes from analysis of the Dependency Map (DepMap) portal[29] (https://depmap.org/portal) (Fig. S2A, B). DepMap-derived genes were chosen by ranking their mean Gene Effect Score (GES), akin to fitness, across all cell lines in DepMap and selecting the highest 100 ("Top Gene Effect Score/TGES") and lowest 50 ("Bottom Gene Effect Score/BGES") CRISPR score-ranked genes, which are predicted to increase or decrease proliferation upon knockout, respectively. The mean Gene Effect Score from the DepMap database is shown by group (Fig. 2B), illustrating the predicted impact of gene knockout on cell viability for each category. The final library comprised 2564 sgRNAs targeting 603 coding regions (3–5 sgRNAs per gene), with an additional 436 control sequences targeting non-exonic regions. sgRNA sequences were retrieved and filtered from a whole-genome CRISPR library[30], then NGS and barcoding adapters were designed and added to the sequences. Subsequently, oligos were synthesized, amplified, and cloned into a lentiviral vector (Fig. S2C, D). Finally, in preparation for the CRISPR screen experiment, library lentivirus particles were produced for MSC transduction.

Using Cas9-expressing bMSCs and a lentiviral sgRNA library, we conducted a CRISPR screen to identify genetic factors influencing cell proliferation. The bMSCs were transduced with the sgRNA library at a low multiplicity of infection (MOI ~ 0.3), ensuring coverage of approximately 600 cells per sgRNA (Fig. S2E). Over a 30-day screening period, cells were passaged every 3–4 days, with DNA samples collected at specified intervals for sgRNA quantification via next-generation sequencing (NGS). sgRNA quantification, ranking, and statistical testing were performed using MAGeCK[31].

A minimum hypergeometric[32] (mHG) analysis of the predefined library sub-groups showed significant enrichment or depletion patterns ($p < 0.001$ | *** | for most days). Gene knockouts enhancing proliferation in the DepMap database, termed TGES, were found to be enriched in the screen, and vice versa, those decreasing proliferation (termed BGES) were depleted (Fig. 2C). Generally, genes that enhance proliferation in human cancer cells (TGES) were similarly enriched in the bovine MSC screen, while genes that reduce proliferation (BGES) were correspondingly depleted, demonstrating consistent functional roles across cell types. Transcription factors showed varied responses: some enhanced proliferation while others were quickly depleted.

To evaluate gene-specific effects on survival and proliferation, we used MAGeCK to calculate fold changes based on the aggregated performance of each gene's 3–5 sgRNAs relative to baseline (day 0; Fig. 2D). This analysis revealed significant shifts in sgRNA abundance over time, identifying candidate proliferation inhibitors such as TP53, PTEN, and VGLL4 ($p < 0.001$ at later time points), whose knockouts increased in abundance, suggesting a growth advantage. In contrast, sgRNAs targeting essential genes for proliferation, including ribosomal proteins and JUN, decreased over time ($p < 0.001$), consistent with reduced cell fitness. Among all candidates, TP53 knockout produced the most pronounced effect, with an over 1000-fold increase in abundance by day 30. This is consistent with TP53 established role as a tumor suppressor that induces cell cycle arrest and senescence in response to stress[33]. PTEN, similarly, acts as a negative regulator of the PI3K/AKT pathway, where its loss leads to increased mTOR activity and can trigger a senescence-like response in some contexts[34]. The enrichment of sgRNAs targeting TP53 and PTEN in our screen supports
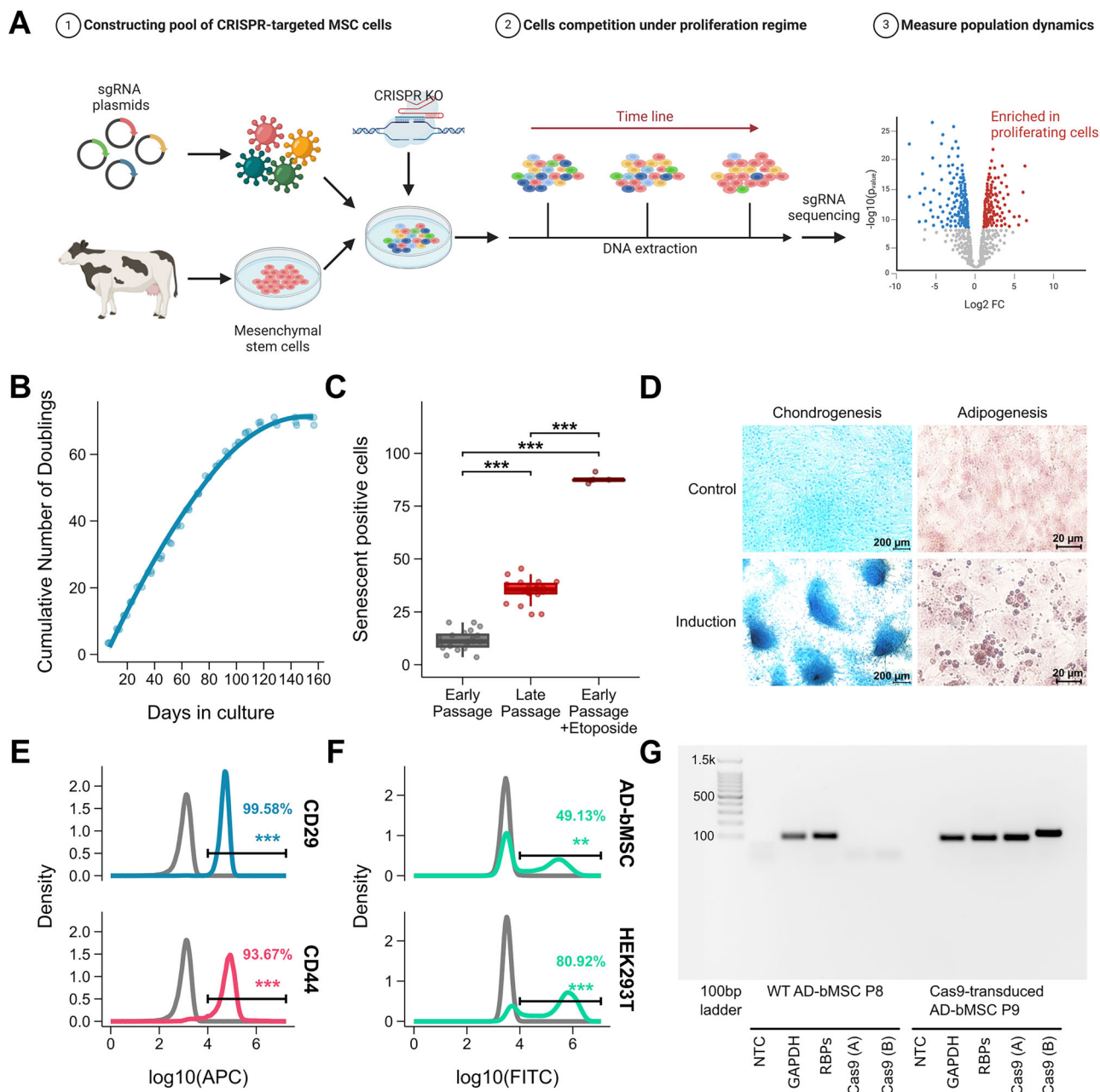
Fig. 1 | Experimental design and characterization of bovine MSCs.
A Experimental design overview of CRISPR-based screening in bovine MSCs.
B Growth kinetics of isolated bMSCs showing consistent cell doubling rate up to 100 days in culture, followed by population doubling arrest, measured by cell counting ($n = 3$). Blue line and shaded envelope represent the fitted linear model and its 95% confidence interval, respectively. **C** Boxplot showing the percentage of senescence-positive cells in early-passage, late-passage, and etoposide-treated early-passage cells. Senescent cells were significantly increased in both late-passage and 20 μM etoposide-treated groups compared to early-passage controls. Each point represents one image field from two biological replicates ($n = 2$). **D** Multi-lineage differentiation potential of bMSCs. Left: Chondrogenesis induced by 21 days in chondrogenic media, visualized by alcian-blue staining of proteoglycans. Right: Adipogenesis induced by 21 days in adipogenic media, visualized by oil-red O staining of lipid droplets. **E** Flow cytometry analysis of bMSCs surface markers CD29 (APC-labeled primary antibody) and CD44 (APC-labeled secondary antibody) at passage 6 ($n = 3$ for each). >90% of the population expresses both markers. Gray plots represent cells stained with secondary antibody only. **F** GFP expression in bMSCs and HEK293T cells following lentiviral transduction. Green histograms represent GFP-transduced cells ($n = 3$), gray histograms show non-transduced control cells ($n = 2$). **G** Cas9 expression in transduced bMSCs assessed by mRNA reverse transcription-PCR, controlled by GAPDH and RPS2 housekeeping genes expression ($n = 2$).

their well-characterized roles in restraining cell growth and highlights their importance in maintaining proliferative homeostasis in MSCs.

Pathway analysis of short-term CRISPR screen identifies five clusters and associated pathways

Building on the insights gained from our initial CRISPR screen, which identified key singular genetic factors influencing cell proliferation, we sought to deepen our understanding by conducting a gene pathway enrichment analysis to identify the regulatory pathways governing the proliferation of AD-bMSCs. This analysis identified five distinct gene clusters based on Spearman's correlation of change over time (Fig. S3A, B). Each cluster exhibited unique abundance patterns over time (Fig. 3A, B). Notably, Cluster 1, which consists of 165 genes with monotonically increasing abundance, was of particular interest for potential enhanced
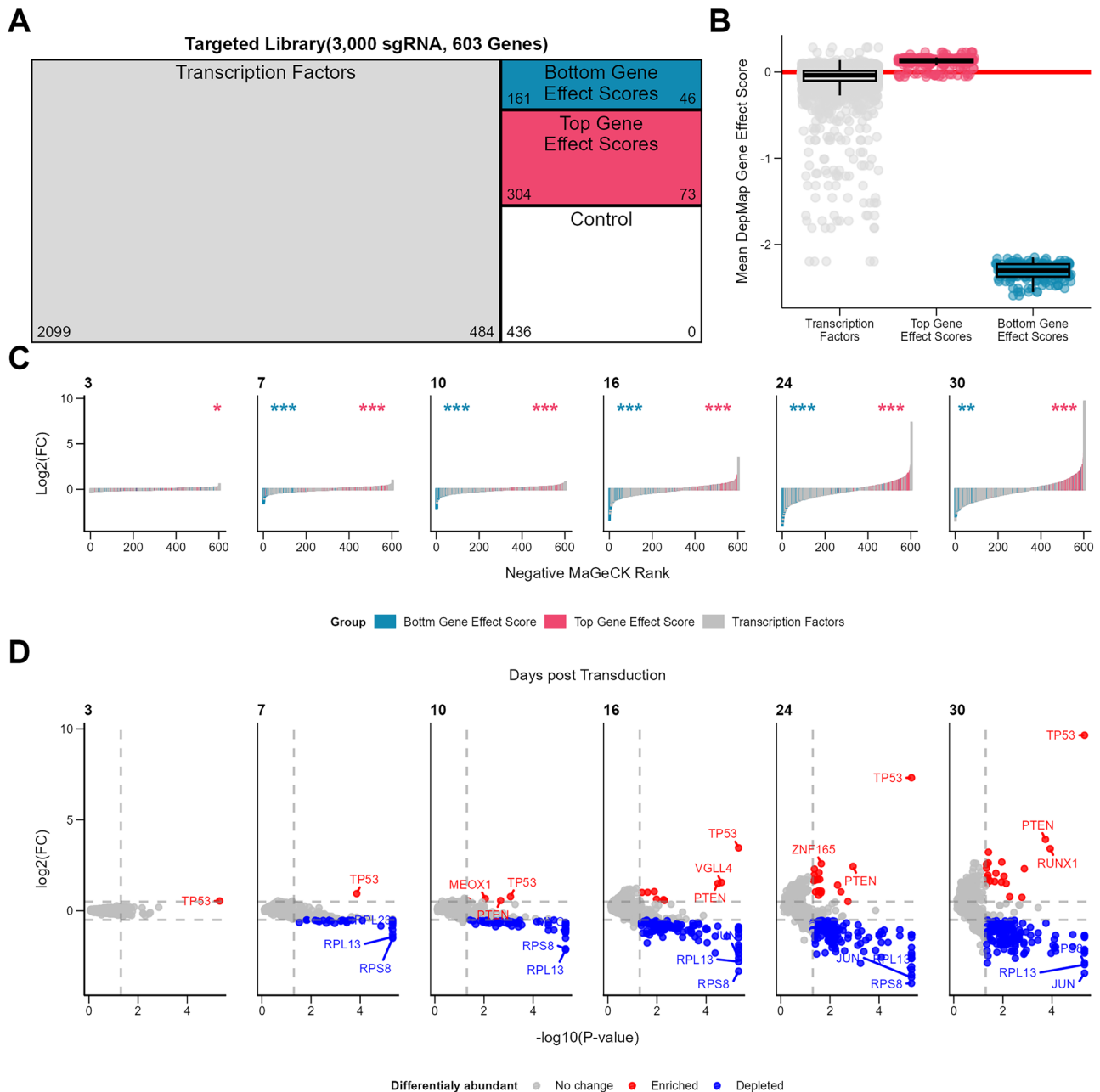
Fig. 2 | CRISPR library design and screening in AD-bMSCs reveals TP53 and PTEN as key regulators of cell proliferation. A Composition of the designed CRISPR sgRNA library. The library consists of 3000 sgRNAs targeting 603 genes, grouped into: Transcription Factors (TF, 2099 sgRNAs/484 genes), Top Gene Effect Score (TGES, 304 sgRNAs/73 genes), Bottom Gene Effect Score (BGES, 161 sgRNAs/46 genes), and controls (436 sgRNAs). **B** Mean Gene Effect Score across all DepMap datasets for each library subgroup, indicating predicted impact on cell fitness upon gene knockout. **C, D** CRISPR screen enrichment analysis. AD-bMSCs were transduced with Cas9-expressing vector followed by the designed sgRNA library ($n = 3$). AD-bMSCs were sampled on days 3, 7, 10, 16, 24, and 30 post-library transduction. **C** Minimum hypergeometric test (mHG) enrichment analysis. Log2 fold-change (y-axis) plotted against log2FC rank (x-axis) over time. Genes with top Gene Effect Scores (TGES) showed significant enrichment (red), while genes with bottom scores (BGES) showed significant depletion (blue). mHG p values are displayed for each day: TGES enrichment (top left, red) and BGES depletion (top right, blue). **D** Volcano plots of screen results by day. $-\log10$ p value (x-axis) plotted against log2 fold-change (y-axis), calculated using MAGeCK. Red: significantly enriched gene-knockouts (leading with *TP53* and *PTEN*); Blue: significantly depleted gene-knockouts; Gray: non-changing gene-knockouts. Dashed lines indicate significance thresholds ($p < 0.05$, $|\log2FC| > 1$).

proliferation. Other significant clusters included Cluster 3, characterized by a decrease in gene abundance, and Cluster 2, which initially decreased followed by an increase. We further characterized these clusters using a ranked over-representation assay (ORA) with the gprofiler2[35] tool to identify enriched Gene Ontology Biological Process (GO:BP) terms (Figs. 3C and S3C). The gene ranking for ORA was determined based on the maximal p value for each gene (Fig. 3C, down). Cluster 1 was significantly enriched with nine GO:BP terms related to proliferation, including three terms associated with TGFβ production and chondrocyte differentiation, processes which are relevant to MSC function and differentiation. These findings suggest potential pathways and gene targets for manipulation to enhance MSC proliferation. However, these findings apply to short-term culturing, and we were also interested in exploring the effects of long-term culturing, particularly through the application of a second CRISPR screen.
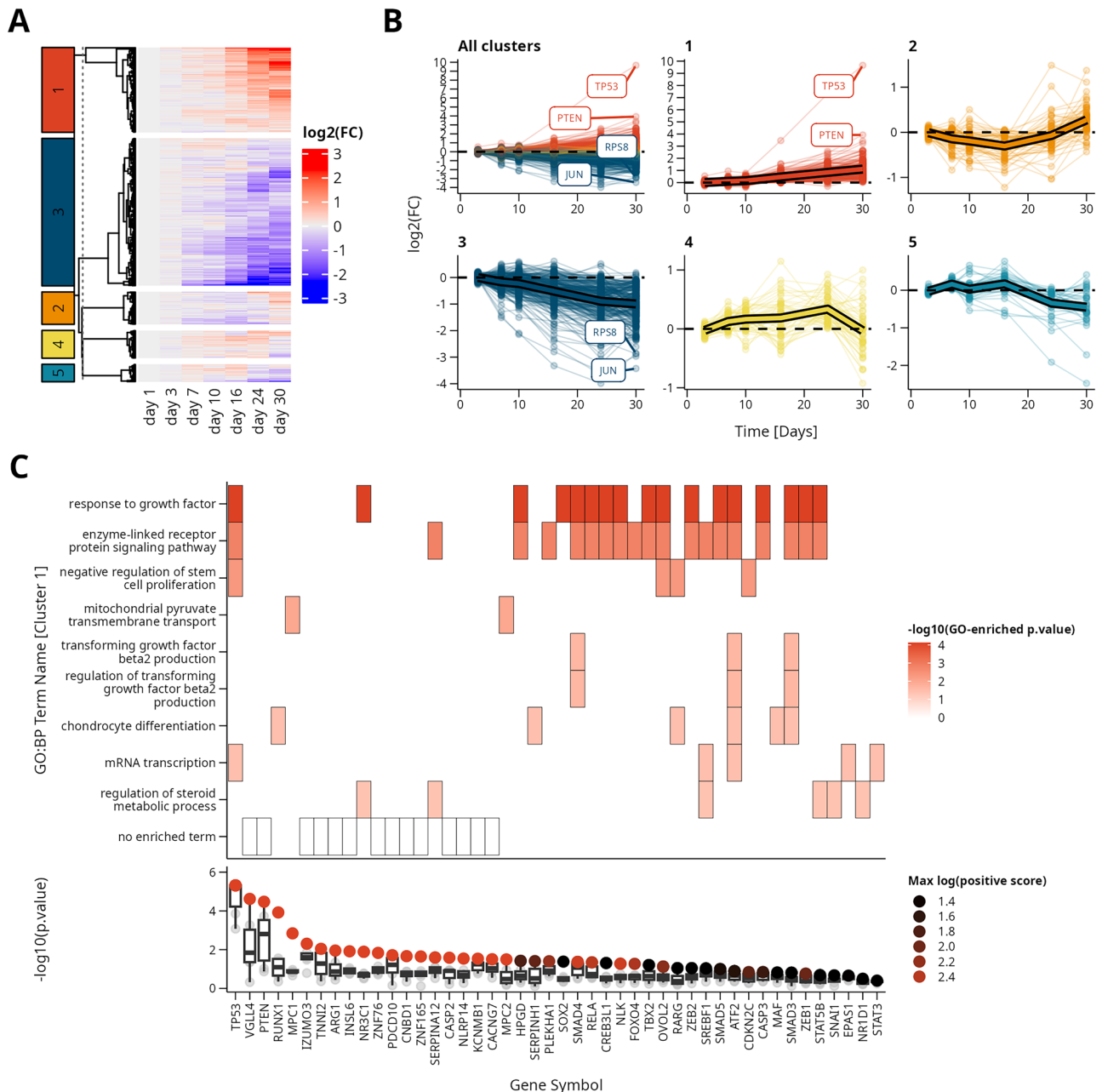
Fig. 3 | Temporal gene expression patterns and functional analysis of CRISPR screen results. A Heatmap showing log2 fold-change trajectories over 30 days for all 603 genes. Red colors represent enriched genes, and blue colors represent depleted genes, with color intensity indicating magnitude of change. Clusters (1–5) correspond to those in (**B**). **B** Mean log2 fold-change (*y*-axis) over time in days (*x*-axis) for five clusters identified by hierarchical clustering: 1 (red): monotonically increasing, 2 (orange): increasing after initial decrease, 3 (dark blue): monotonically decreasing, 4 (yellow): decreasing after initial increase, 5 (light blue): non-monotonically decreasing. Each thin transparent line represents one gene. Thick black-outline lines represents the mean for each cluster. **C** Functional analysis of genes with consistently increasing abundance (Cluster 1): (Top) Gene Ontology (GO) enrichment analysis: Significantly enriched biological processes (*y*-axis) and their key contributing genes (*x*-axis). Color intensity indicates −log10(*p* value) of GO term enrichment. (Bottom) Gene ranking based on MAGeCK analysis: Genes (*x*-axis) ranked by −log10(*p* value), with color intensity indicating a more positive enrichment score. These pathways may enhance proliferation when perturbed.

CRISPR long-term proliferation screen highlights *TP53* as the top candidate for knockout-mediated proliferation-enhancement

To investigate regulators that enable prolonged cell division and bypass senescence, we performed a second CRISPR screen over 200 day period, compared to the initial 30-day screen. bMSCs were transduced with Cas9 and the sgRNA library at a higher multiplicity of infection (MOI). Two control groups were included: untransduced cells and cells transduced with Cas9 only. The total culture duration before proliferation arrest increased from about 100 days in wild-type cells to approximately 200 days in transduced cells, effectively extending the proliferation period after controls stopped dividing (Fig. 4A). Transduced cells also showed faster proliferation, with an average 12% increase in doubling rate and up to a 50% increase by day 50 post-transduction compared to non-transduced controls (Fig. 4B). To determine whether the decline in proliferation was associated with senescence, we performed SA-β-gal staining at day 80, comparing Cas9-transduced cells with the sgRNA library (+library) to those without the library (−library) (Fig. 4C). The −library group showed a significantly higher rate of senescence, with ~60% senescent cells, compared to only ~10% in the +library group. This suggests that the extended proliferative capacity at later time points in the +library group is largely due to a reduced rate of senescence.
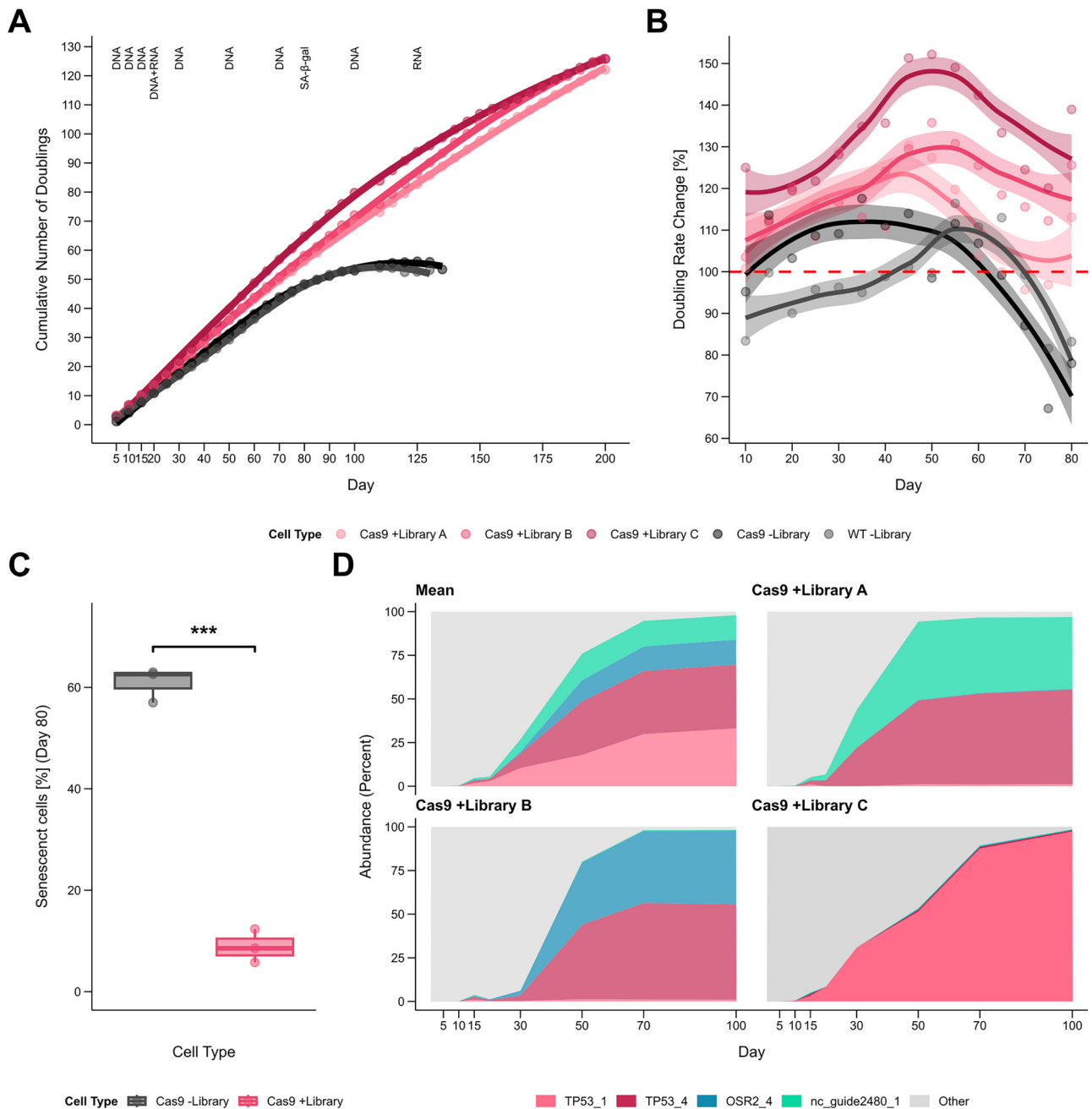
Fig. 4 | Long-term proliferation and sgRNA dynamics in CRISPR-edited AD-bMSCs. AD-bMSCs were transduced with Cas9 and the sgRNA library, then cultured for 200 days with DNA sampling every 5 days and RNA sampling at days 20 and 125. **A, B** Proliferation kinetics of sgRNA-library-transduced cells (red, $n = 3$) compared to un-transduced (gray) and Cas9-only transduced cells (black). Proliferation was measured by direct cell counting at each passage. **A** Doubling time in hours over the course of the experiment. **B** Cumulative number of doublings since the start of the screen. **C** Boxplot showing the percentage of senescence-positive Cas9 +library cells compared to Cas9 −library cells at day 80. Non-library cells had increased senescent rate compared to library cells. Each point represents biological replicate ($n = 3$). Shaded areas indicate the 95% confidence interval. **D** Relative abundance of sgRNAs over 100 days across three biological repeats: Top-left: Mean abundance of the top 4 sgRNAs (red, blue, and green) and all other sgRNAs (gray). Remaining panels: Individual abundance trajectories for each biological repeat.

Sequencing DNA from multiple time points revealed significant shifts in sgRNA abundance beginning at day 25, with *TP53*-targeting guides showing a pronounced and consistent enrichment (Fig. 4D). In replicate C, *TP53* sgRNAs became nearly fixed in the population (>99%), while in replicates A and B, they accounted for approximately 50%. The remaining sgRNAs were primarily those targeting *OSR2* in replicate B and a non-cutting control (nc2480) in replicate A. Notably, *OSR2* was previously depleted in the short-term screen, and nc2480 is designed not to impact cellular function. The mirrored enrichment of these guides alongside *TP53* is likely the result of co-inheritance due to high multiplicity of infection

(MOI) during lentiviral transduction, rather than independent selective advantages. Thus, the apparent enrichment of *OSR2* and nc2480 likely reflects technical artifacts rather than true biological effects. Despite these complexities, *TP53* consistently emerged as the dominant and most robust candidate for enhancing proliferation following knockout.

RNA sequencing of the CRISPR long-term proliferation screen identifies key genes and pathways
To further understand the regulatory mechanisms governing AD-bMSCs proliferation, we extracted and sequenced RNA from early wildtype
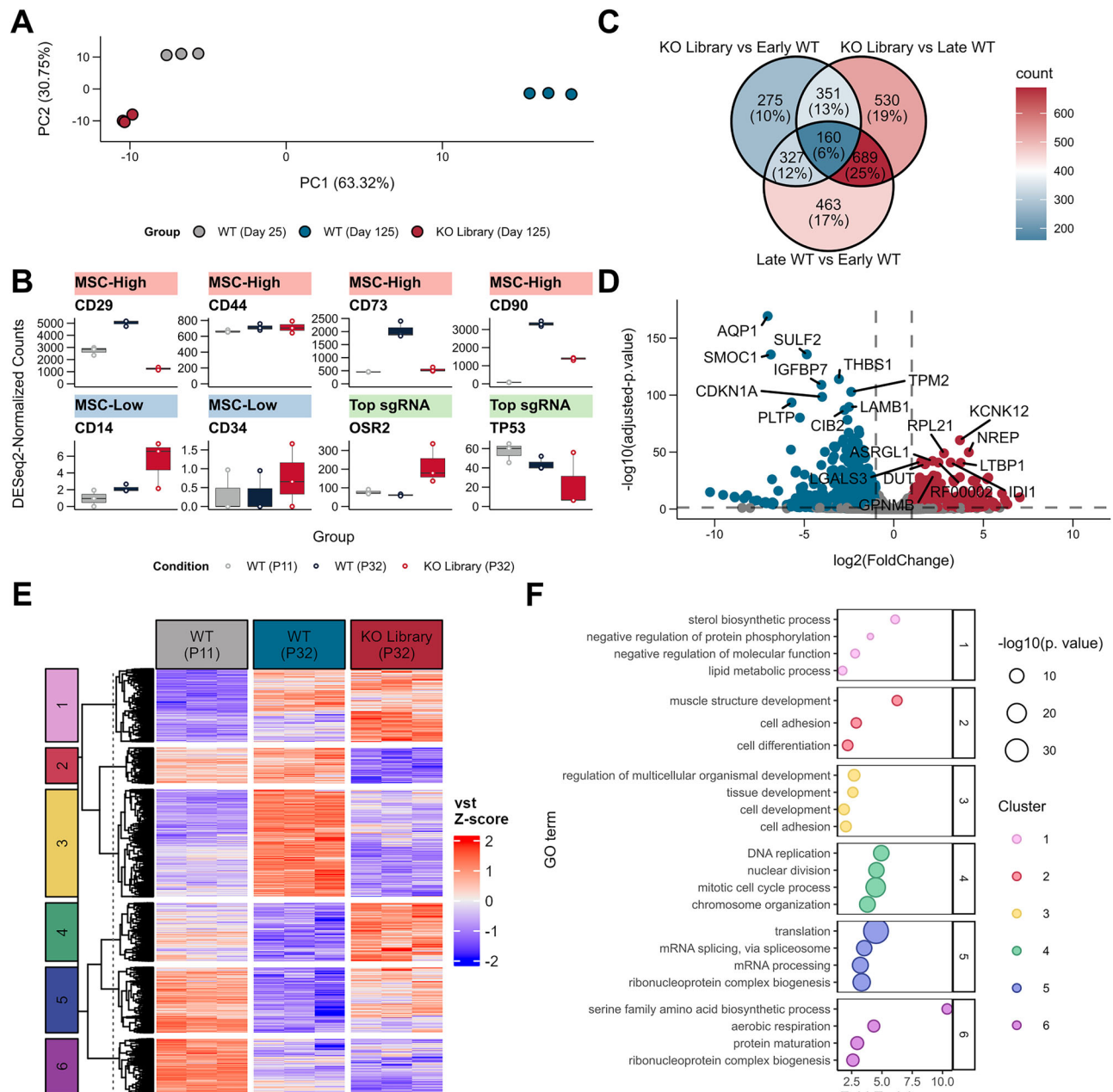
Fig. 5 | Transcriptomic analysis of wildtype and CRISPR-modified AD-bMSCs at different passages. A Principal component analysis (PCA) of RNA-seq samples, showing KO Library (day 125) cells clustering closer to WT (day 25) than to WT (day 125). **B** Boxplot of normalized RNA-seq reads (*y*-axis) by cell type (*x*-axis) for 8 selected genes, categorized into three groups: positive MSC markers (red), negative MSC markers (blue), and candidate genes from Fig. 4 (TP53 and OSR2, green). **C** Venn diagram of all differentially expressed genes, grouped by group comparison. **D** Volcano plot showing −log10(*p* value) vs. log2 fold change for genes differentially expressed in KO Library (day 125) compared to Late WT (day 125). Red points indicate enriched genes, blue points indicate depleted genes. **E** Heatmap of differentially expressed genes (DEGs, rows) across the three replicated of the three groups (columns). Values represent variance stabilizing transformed (VST) and *Z*-score scaled RNA-seq counts. DEGs are clustered into six groups (1–6) using hierarchical clustering. **F** Top 4 enriched Gene Ontology (GO) Biological Process category terms for each cluster. *Y*-axis: GO terms; *X*-axis: Fold enrichment. Rows represent different clusters. Point size corresponds to −log10(*p* value) of the enrichment.

(WT) passage cells (day 25), late passage cells (day 125), and sgRNA library-transduced cells (KO Library, day 125) collected on the mentioned days of the second CRISPR screen (Fig. 4B). Principal component analysis (PCA) revealed that late-passage KO library cells (KL) retained similarity to early-passage WT cells (EWT), while late-passage WT (LWT) cells diverged (Fig. 5A, see also Fig. S4), with this difference accounting for most of the variance (63%). We examined the expression levels of known MSC markers and candidate genes identified in the previous CRISPR screen (Fig. 5B). Both LWT and KL cells expressed positive MSC markers at levels similar to or higher than EWT, except for

a lower expression of CD29 in KL cells. Negative MSC markers were slightly elevated in KL cells but remained low overall, indicating that KL cells retained some MSC expression profile even at late passages. Differential expression analysis using DESeq2 between all three groups identified differentially expressed genes (DEGs, Fig. 5C). Specific comparison of KL and LWT cells reveals genes that may contribute to KL cells' enhanced proliferation and younger expression profile (Fig. 5D, see also Fig. S5). Top DEGs include upregulated genes like KCNK12, NREP, IDI1, and LTBP1, and downregulated genes such as AQP1, SMOC1, SULF2, THBS1, and PLTP. Hierarchical clustering of gene expression

profiles revealed six distinct clusters (Fig. 5E). Over-representation analysis of GO:BP terms for each cluster identified cluster-specific pathways and terms (Fig. 5F). Key findings included sterol and lipid metabolism for cluster 1 (up-regulated in both KL and LWT), differentiation and cell adhesion terms for cluster 2 and 3 (downregulated in KL cells), DNA and cell-cycle terms for cluster 4 (upregulated in KL), and protein synthesis-related terms for clusters 5, 6 (downregulated in LWT cells). Our findings suggest that KL cells' increased proliferation and extended culturing time may be attributed to upregulated cell-cycle and DNA replication genes (cluster 4) and maintained protein-synthesis gene expression levels similar to EWT (Cluster 5). Despite these changes, KL cells downregulate differentiation related genes, and specifically muscle-differentiation, indicating that *TP53* knockout might inhibit muscle-directed or differentiation, or differentiation of MSCs in general.

Validation of *TP53* and *PTEN* knockouts

To validate the results of the pooled CRISPR screen, *TP53* and *PTEN*, the top candidate genes, were individually knocked out in bMSCs using Cas9 and gene-specific sgRNAs, alongside a non-targeting sgRNA control. Following transfection and 1 week of selection, two single-cell clones from each knockout pool were isolated by serial dilution. Cell viability, assessed by Alamar Blue assay (Fig. 6A), was significantly higher in both *TP53* and *PTEN* knockout (KO) populations compared to wild-type (WT) cells ($p < 0.01$). Flow cytometry confirmed that KO cells retained MSC surface marker expression (CD29, CD44) at levels comparable to WT (Fig. 6B), while the non-targeting control showed reduced expression, possibly due to off-target or sgRNA-related effects. Genome editing efficiency, measured by sequencing and indel analysis, reached 95% in *TP53* KO and 43% in *PTEN* KO cells, with most edits resulting in frameshifts (Fig. 6C). qRT-PCR further confirmed strong knockdown of target gene expression in two independent single-cell clones per gene (Fig. 6D). Adipogenic differentiation was assessed via BODIPY (lipid) and Hoechst (nuclei) staining after 21 days in induction medium (Fig. 6E). The percentage of BODIPY-positive cells was reduced in both knockouts dropping from 67.8% in WT to 37.7% in *TP53* KO and 25.5% in *PTEN* KO (Fig. 6F). However, Hoechst-based total cell counts increased in three of the four KO lines, with the fourth similar to WT (Fig. S6), suggesting that the reduced proportion of adipogenic cells may partly reflect ongoing proliferation, which increases total cell number, rather than a complete loss of differentiation capacity. Senescence, assessed by SA-β-gal staining (Fig. S6), was comparable between WT and knockouts. Notably, *TP53* KO cells exhibited a higher absolute number of cells, consistent with their overall increase in cell number. In summary, targeted knockout of *TP53* or *PTEN* enhances bMSC proliferation without increasing senescence, but reduces adipogenic differentiation efficiency. While this tradeoff may not preclude their application in cultured meat, further optimization is needed to balance expansion and differentiation potential. These results validate the CRISPR screen and underscore the utility of gene editing to improve MSC-based cultured meat production.

Discussion

Slow proliferation and early senescence limit the scalability of bovine mesenchymal stem cells (bMSCs) for cultured meat production. To tackle those challenges, we conducted a CRISPR-based functional genomics screen in bMSCs, targeting proliferation with a library of 603 gene knockouts. We discovered that inactivating *TP53* and *PTEN* genes most significantly enhanced bMSC proliferation and delayed cellular senescence. These results directly address slow cell expansion as a major obstacle in cultured meat production by providing a genetic approach to shorten timelines and lower costs for industrial-scale manufacturing[16]. The prominence of these well-established tumor suppressors as top hits provides a foundation for cell line engineering but necessitates careful consideration of the mechanisms and safety implications of their manipulation.

Specifically, *TP53* knockout significantly increased proliferation, maintained early-passage gene expression, and extended population doublings by delaying senescence onset. This aligns with *TP53*'s well-

established role as a key regulator of senescence, apoptosis, and DNA repair[33], as well as its frequent identification in CRISPR knockout screens across diverse cell lines[36]. Proliferation is thus enhanced via two complementary mechanisms: accelerating cell division to produce more cells in less time, and postponing senescence to prolong the proliferative lifespan, resulting in a greater overall cell yield. Similarly, *PTEN* knockout emerged as a strong candidate due to its involvement in cell cycle regulation and apoptosis[37], although its effects on senescence appear context-dependent[34]. Nonetheless, these proliferative gains often come with trade-offs in differentiation potential.

Balancing proliferation with differentiation potential is therefore essential for optimizing MSCs for cultivated meat applications[38]. Although prior studies have linked *TP53* knockout to enhanced adipogenic differentiation[39–41], we found that both *TP53* and *PTEN* knockouts reduced the proportion of adipogenic cells. However, the total number of adipogenic cells was less affected, likely because undifferentiated cells with a proliferative advantage outcompeted differentiating ones. Similarly, *TP53* knockout populations showed downregulation of muscle-related genes, suggesting diminished myogenic potential[21] and posing limitations for cultured muscle production. While this study focuses on adipogenic-competent MSCs for fat tissue applications, cell lines intended for myogenic differentiation will require independent validation to ensure that proliferation-enhancing modifications do not impair muscle development and function.

Beyond *TP53* and *PTEN*, our screen uncovered additional gene knockouts that may promote proliferation through distinct metabolic and signaling mechanisms. Knockout of mitochondrial pyruvate carrier[42] (*MPC1* and *MPC2*) subunits increased cell abundance, suggesting proliferative advantages through metabolic shifting toward aerobic glycolysis[43,44] a shift associated with mitochondrial involvement[45,46]. Similarly, knockouts of *SMAD3*, *SMAD4*, and *SMAD5* increased bMSC abundance, highlighting their involvement in TGF-β and BMP signaling pathways that govern chondrogenesis[47]. Notably, disrupting chondrogenesis-associated genes (e.g.,: *SMADs*, *RUNX1*[48] and *SERPINH1*[49]) may accelerate proliferation while reducing undesired cartilage differentiation, providing dual benefits for cultivated meat production.

Building on these findings, this CRISPR screening framework can be readily adapted to other phenotypes[50] and cell sources[17] critical for cultivated meat production, including satellite cells, embryonic stem cells, and induced pluripotent stem cells, which can be combined to produce cultured meat products. Future screens could interrogate adipogenic and myogenic differentiation, reduced serum dependence, and growth in suspension culture, identifying novel regulators of lineage commitment and metabolic adaptation.

The use of CRISPR-edited cells in food production raises important safety and regulatory challenges. Extended culturing of cells with tumor-suppressor knockouts may induce genomic instability, necessitating careful monitoring[51]. For large-scale production, transient gene modulation using chemical inhibitors or inducible systems may be safer than permanent genetic edits. However, only compounds with established safety profiles (e.g., GRAS status in the U.S. or EFSA approval in Europe) are likely suitable for food applications. While CRISPR does not necessarily introduce foreign DNA, regulatory frameworks in many countries consider it as genetic modification, requiring strict oversight and potentially facing consumer skepticism[52]. Future implementation will require careful selection of approved compounds, validation of their removal from products, and transparent safety testing to ensure consumer trust and regulatory compliance across global markets.

Future research should prioritize evaluating both the safety and functionality of these modified bMSCs in food systems, while also exploring combinatorial approaches to further improve efficiency. The versatility of CRISPR technology offers opportunities to systematically optimize cell lines for scalable biomanufacturing, with interdisciplinary collaboration being crucial for advancing sustainable alternatives to conventional meat production.
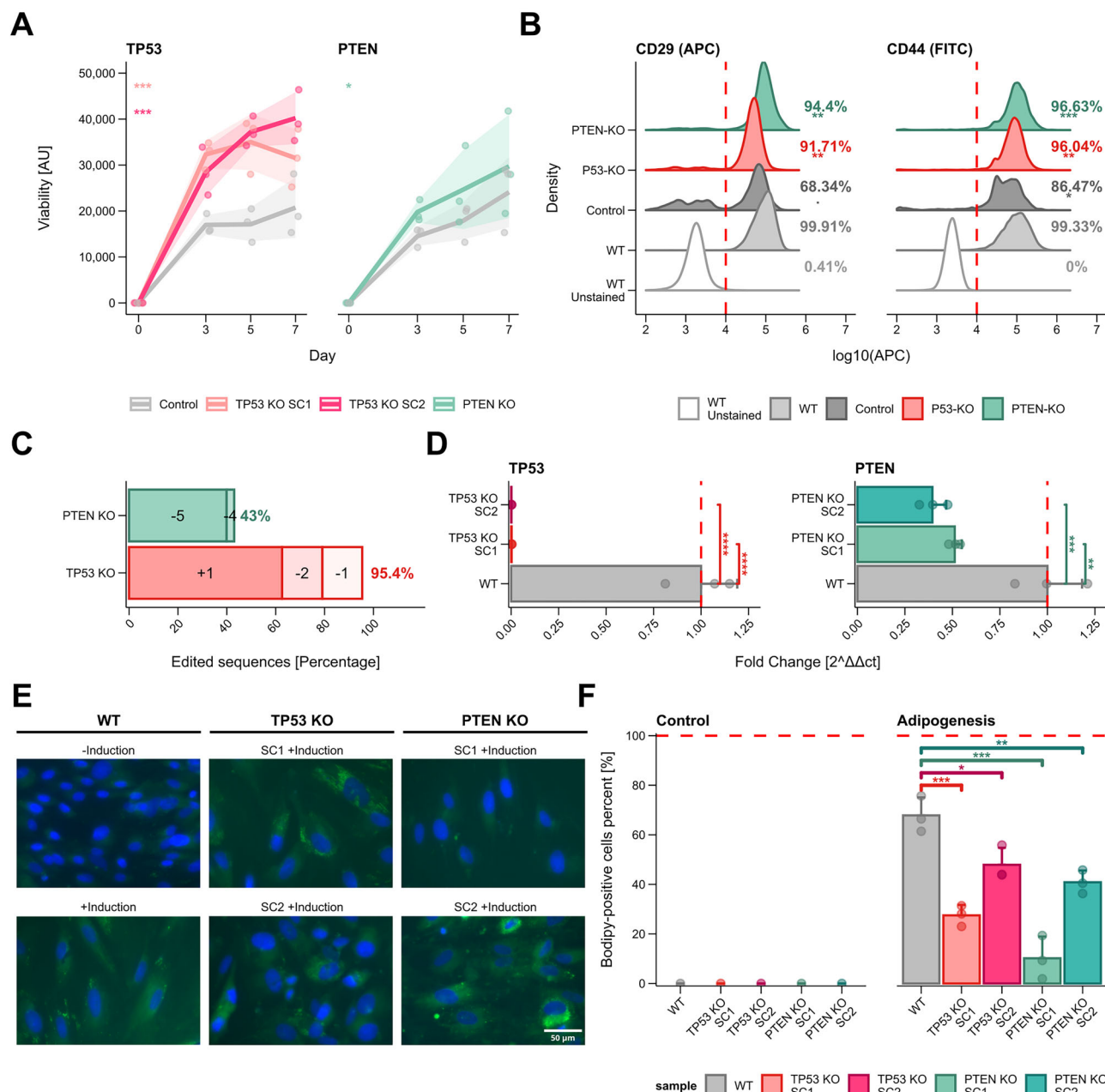
Fig. 6 | Validation of *TP53* and *PTEN* knockouts in AD-bMSCs. AD-bMSCs were transfected with Cas9 and an sgRNA targeting either *TP53* (red), *PTEN* (green), or a non-exonic targeting control sgRNA (gray) (*n* = 3 per group). **A** Cell viability was measured using the Alamar Blue assay at days 3, 5, and 7 after seeding. Both *TP53* and *PTEN* knockout cells exhibited significantly increased viability compared to wild-type (WT) controls. Shaded areas indicate the 95% confidence interval. **B** Flow cytometry analysis of surface markers CD29 (APC) and CD44 (FITC) in bMSCs. *TP53* and *PTEN* knockout cells maintained surface marker expression levels similar to WT cells, while the control group showed a minor reduction. **C** Editing efficiency and indel distribution in knockout populations, as determined by next-generation sequencing. Bars represent the percentage of sequences with specific insertions (+) or deletions (−). *TP53* knockout cells showed 95% editing efficiency, while *PTEN* knockout cells showed 43%. **D** qRT-PCR analysis of *TP53* and *PTEN* mRNA expression in knockout and WT cells, normalized to the RBPs housekeeping gene. Two independent single-cell clones (SC) for each knockout showed significant reductions in target gene expression. **E** Representative fluorescence microscopy images showing adipogenic differentiation after 21 days in induction medium. Lipid droplets were stained with BODIPY (green), and nuclei with Hoechst (blue). **F** Quantification of adipogenic differentiation efficiency, expressed as the percentage of BODIPY-positive cells. Both *TP53* and *PTEN* knockout clones showed a significant reduction in adipogenic potential compared to WT. Statistical significance is indicated (*$p < 0.05$, **$p < 0.01$, ***$p < 0.001$).

Online methods

Bovine MSC isolation and characterization

This section outlines the isolation of adipose-derived bovine MSC (AD-bMSCs) from calf tissue, their culture methods, and characterization procedures. We describe the process for cell isolation, the expansion and maintenance of AD-bMSCs in culture, and the analysis of their growth kinetics. Additionally, we detail the flow cytometry methods used to confirm MSC-specific surface markers, and the differentiation assays employed to verify multipotency. These procedures collectively establish the identity and quality of the AD-bMSCs used in subsequent CRISPR screening experiments.

AD-bMSCs isolation

AD-bMSCs were isolated from 3-month-old female calves immediately post-slaughter, following a modified protocol from Sampaio et al.[27]. Briefly,

adipose tissue was aseptically collected and washed with phosphate-buffered saline (PBS; Biological Industries, Israel) containing Pen-Strep Solution (Biological Industries). The tissue was surface sterilized with 75% ethanol for 30 s. Blood vessels and connective tissues were meticulously removed, and the adipose tissue was minced into small pieces before being digested with Collagenase type I solution (2 mg/mL in DMEM/LG; Worthington, USA) at a 1:10 ratio for 3 h at 37 °C. The enzymatic reaction was terminated by adding an equal volume of Dulbecco's Modified Eagle's Medium Low Glucose (DMEM/LG; Biological Industries) supplemented with 15% fetal bovine serum (FBS; Biological Industries). The digested product was filtered through a 200-μm mesh sieve and centrifuged at $300 \times g$ for 10 min. The resulting cell pellet was resuspended in culture medium and seeded in 10 cm² dishes. Cells were incubated at 37 °C in a 5% CO_2 atmosphere. After 24 h, non-adherent cells were removed by washing with PBS. When the cells reached 80% confluence, they were passaged using trypsin (Biological Industries, Israel).

AD-bMSCs routine culturing
AD-bMSCs were expanded in low-glucose DMEM supplemented with 15% fetal bovine serum (FBS), 2 mM L-glutamine, and 1% Pen-Strep X100 (final concentrations: 100 units/mL Penicillin G Sodium Salt, 0.1 mg/mL Streptomycin Sulfate) (Sartorius). Cells were maintained in a humidified incubator at 37 °C with 5% CO_2 and passaged every 3–4 days at 60–80% confluency using 0.25% Trypsin Solution A (Sartorius). For cryopreservation, cells were counted, centrifuged at $400 \times g$, and resuspended in full growth medium containing 10% DMSO v/v (Sigma-Aldrich, Israel). Cryovials were initially stored at −80 °C for short-term preservation, then transferred to liquid nitrogen for long-term storage.

Cell culture and growth kinetics
Growth kinetics were analyzed for AD-MSCs from thirteen different replicates, spanning passages 3 through 25. Cells were seeded in multi-well plates or 10 cm cell dishes at a density of approximately 7000 cells/cm² and maintained in MSC culture medium at 37 °C in a humidified atmosphere with 5% CO_2. The medium was refreshed every 48 h. Cells were passaged and counted every 96 h (coinciding with every other medium replacement). Briefly, cells were trypsinized, stained with trypan blue, and viable cells were counted using a Countess II hemocytometer (Thermo Fisher Scientific, USA). Population doubling time (Td) during the logarithmic growth phase was calculated using the Patterson formula:

$$Td = t \times lg2 / (lgnt - lgNo)$$

Where: t = incubation time, No = initial cell number, Nt = cell number at time t.

Senescence-associated β-gal (SA-β-gal) staining
To assess the percentage of senescent cells in AD-bMSCs, SA-β-gal staining was performed using the Senescence β-Galactosidase Staining Kit (Cell Signaling Technology, #9860), following the manufacturer's instructions. Briefly, cells were seeded at a density of 1×10^4 cells/cm². After 24 h, 20 μM etoposide (Abcam, AB-ab120227-25-B) was added to the relevant treatment groups. Cells were subsequently washed once with PBS and fixed with the provided Fixative Solution for 15 min in a chemical hood. Following fixation, cells were washed twice with PBS and incubated with the Staining Solution. Plates were sealed with parafilm and incubated in a dry 37 °C incubator (no CO_2) for at least 24 h. After staining, cells were imaged, and senescent cells were manually annotated and counted.

Differentiation assays
Adipogenic differentiation. AD-bMSCs were subjected to adipogenic differentiation for 14 days using an alternating induction and maintenance medium protocol. The induction medium consisted of Low-glucose DMEM supplemented with 10% FBS, 1% penicillin/streptomycin, 1% L-glutamine, 1 μM dexamethasone, 0.5 mM 3-isobutyl-1-methylxanthine, 0.2 mM indomethacin, and 10 μg/mL insulin (all from Sigma-Aldrich). Cells were cultured in this medium for 3 days, followed by 1 day in maintenance medium (DMEM-LG, 10% FBS, 1% penicillin/streptomycin, and 10 μg/mL insulin). This cycle was repeated for the duration of the experiment. Control cells were maintained in standard growth medium. After 14 days, adipogenic differentiation was quantified via lipid content as assessed by either Oil Red O (ORO) staining or BODIPY staining (Invitrogen). For ORO staining, cells were washed twice with PBS and fixed with 4% formaldehyde for 10 min at room temperature. Fixed cells were then incubated for 1 h with freshly prepared ORO working solution (6 parts 0.5% ORO stock solution in isopropanol mixed with 4 parts distilled water). Cells were then washed thoroughly with distilled water before imaging. For BODIPY imaging, cells were washed twice with PBS, and then imaged.

Chondrogenic differentiation. AD-bMSCs at passages 9 were induced to undergo chondrogenic differentiation for 21 days. The chondrogenic medium (CM) consisted of DMEM/F12 supplemented with 10% FBS, 1% insulin-transferrin-selenium (ITS), 50 μg/mL proline, 0.1 μM dexamethasone, 0.9 mM sodium pyruvate, 50 μg/mL L-ascorbic acid, and 10 ng/mL transforming growth factor β3. The culture medium was replaced every 3 days. Chondrogenic differentiation was evaluated by Alcian Blue staining to detect glycosaminoglycan (GAG) production. After 21 days, cells were fixed in cold methanol for 5 min, then incubated in 1% Alcian Blue solution (pH 2.5) for 30 min at room temperature. Cells were then washed three times with PBS before imaging.

Flow cytometry analysis
Flow cytometry was performed on AD-bMSCs at different passages to investigate the expression of MSC-specific markers CD29 and CD44. AD-bMSCs were harvested using 0.25% trypsin-EDTA. The cell suspension was centrifuged at $300 \times g$ for 5 min and washed three times with DPBS containing 1% bovine serum albumin (Sigma-Aldrich). The AD-bMSCs were filtered through a 70-μm nylon cell strainer, and cell concentration was determined using a hemocytometer. Approximately 5×10^5 cells per sample were labeled with FITC-conjugated anti-bovine CD44 antibody (1:250 dilution, Catalog #AB_528148, DSHB) and incubated at 4 °C in the dark for 30 min. In parallel, an equal number of cells were directly labeled with APC-conjugated anti-bovine CD29 antibody (1:250 dilution, Catalog #303008, BioLegend). All samples were washed twice with PBS and centrifuged at $300 \times g$ at 4 °C for 5 min. The washed cells were resuspended in 200 μL of PBS and filtered through a 100-μm nylon cell strainer. Labeled samples were analyzed using a BD Accuri™ C6 Plus Flow Cytometer. For each sample, at least 10,000 events were recorded. Data analysis and plot generation were performed using R with packages flowCore and ggcyto (see "Bioinformatics" section for details). Positive expression was defined as fluorescence intensity greater than 99% of the corresponding unstained control.

Cas9 mRNA expression validation in transduced cells
RNA was extracted and amplified from Cas9-transduced cells to verify mRNA expression. Total RNA was isolated from 5×10^6 cells using TRIzol reagent (Invitrogen), followed by purification with the Direct-zol RNA Miniprep Plus Kit (Zymo Research). cDNA was amplified using Taq Mix Red (PCRBIO) according to the manufacturer's instructions. PCR products were run on a 2% agarose gel and visualized using a UV transilluminator. Primer sequences are found in Table S1.

Reporting summary
Further information on research design is available in the Nature Portfolio Reporting Summary linked to this article.

CRISPR library construction and screening
This section outlines the design and construction of a custom CRISPR library targeting key genes involved in cell cycle regulation, cloned into a lentiviral vector system that co-expressed Cas9. Following lentiviral

production and transduction, the bMSCs population was cultured under proliferative conditions. Genomic DNA was extracted at various timepoints for next-generation sequencing (NGS) analysis, enabling the identification of genes whose knockout enhanced bMSCs proliferation while preserving differentiation capacity.

CRISPR library design

We designed a focused CRISPR knockout library targeting 603 Bos taurus genes related to proliferation, including transcription factors and genes selected from the Dependency Map (DepMap) portal based on their Gene Effect Scores. The library comprised 2564 sgRNAs targeting coding regions and 436 control sequences. sgRNA sequences were retrieved and filtered from a previously published whole-genome CRISPR library, with NGS, barcoding adapters, and restriction enzyme recognition site added to the sequences. Detailed information on gene selection criteria and library composition is provided in the "Results" section.

Library oligonucleotide synthesis, amplification and cloning

The custom CRISPR library was synthesized as an oligonucleotide pool by Twist Biosciences. Upon receipt, the lyophilized pool was reconstituted in TE buffer to a concentration of 1 ng/μL. Single-stranded oligos were PCR-amplified using universal library adapter primers in triplicate. The amplified products were combined, purified using the Promega Wizard® SV Gel and PCR Clean-Up System, and verified on a 2.5% agarose gel. Concentration was determined using both NanoDrop and Qubit instruments. The amplified library was inserted into LentiGuide-Puro (Addgene #52963) using a GoldenGate reaction with BsmbI/Esp3I enzymes, following a modified protocol based on Read et al. Oligonucleotide sequences are found in Table S2.

Bacterial transformation and library amplification

Ligation products were purified by ethanol precipitation and resuspended in 5 μL TE buffer. One microliter of purified ligation product was electroporated into 50 μL of either NEB Stable or Lucigen Endura electrocompetent cells using a Gene Pulser Xcell Electroporation System (Bio-Rad) at 1800 V, 600 Ω, and 10 μF. post-electroporation, bacteria were recovered in 1 mL SOC medium for 1 h at 37 °C with 250–300 RPM shaking. Each 1 mL of recovered bacteria was split 10%:90%; the 10% fraction was used for serial dilution plating and colony counting, while the 90% fraction was amplified for plasmid library extraction. Colony forming units (CFUs) were determined by plating dilutions of $1:2 \times 10^5$, $1:2 \times 10^6$, and $1:2 \times 10^7$ on ampicillin-containing agar plates. Library coverage was calculated, with a minimum threshold of 1000 CFUs per sgRNA. For plasmid library amplification, the 90% fraction of recovered bacteria was diluted into 250 mL LB + ampicillin and grown at 25 °C and 250–300 RPM for at least 16 h until OD ≥ 1. Approximately 10 aliquots of 1 mL bacteria were cryopreserved with 25% glycerol. The remaining culture was used for plasmid DNA extraction using "NucleoBond Xtra Midi" (MACHEREY-NAGEL), with final elution in 500 μL. Plasmid concentration and purity were determined by NanoDrop.

Lentiviral production

The following lentivirus-production related plasmids were amplified in bacteria and extracted using "NucleoBond Xtra Midi" as per manufacturers instruction: Second-generation lentiviral envelope and packaging plasmids (VSV-G envelope pMD2.G, Addgene #12259; psPAX2, Addgene #12260), a control lentiGFP plasmid, and two CRISPR-Cas9 plasmids (Lenti-iCas9-neo, Addgene #85400; lentiCas9-Blast, Addgene #52962) were amplified in bacteria and extracted using standard plasmid midi-prep protocols. For transfection, a mix of VSV-G/psPAX2/Transfer vector was prepared at a ratio of 3:1:4 and introduced into HEK293T cells using TurboFect (Rhenium) reagent as per manufacturers instruction. The medium was replaced with complete HEK293T medium 24 h post-transfection. Lentiviral particles were harvested 48–72 h post-transfection by collecting the cell culture medium and centrifuging at $400 \times g$ at 4 °C for 5 min to remove cellular debris. The supernatant was supplemented with 10 mM HEPES buffer to stabilize pH, filtered through a 0.45 μm PES filter, aliquoted, and snap-frozen in liquid nitrogen before storage at −80 °C.

Lentiviral transduction optimization via flow cytometry analysis

MSCs were transduced with GFP vector-containing lentivirus to assess transduction efficiency. Cells were seeded in 6-well plates at a density of 1.5×10^5 cells per well 24 h prior to transduction, or on the day of transduction for reverse transduction. Lentiviral particles were added to the cells at various multiplicities of infection (MOI), in the presence of different transduction enhancers (8 or 4 μg/mL polybrene, 10 or 5 μg/mL protamine sulfate, or 1X ViralEntry). Both forward and reverse transduction methods were tested. For reverse transduction, virus and enhancers were mixed with cells upon seeding. Cells were incubated with virus for 24 h, after which the media was replaced with fresh growth media. GFP expression was analyzed 72 h post-transduction by splitting and washing the cells, then measuring GFP intensity using a BD Accuri C6 flow cytometer. A minimum of 10,000 events were collected for each sample. Data were analyzed using R flowCore package to determine the percentage of GFP-positive cells and mean fluorescence intensity.

Lentiviral transduction and titration

Transduction was performed using a reverse transduction method. Cells were passaged, counted, and resuspended in fresh low-glucose DMEM supplemented with varying concentration of transduction enhancers (Polybrene, Protamine sulfate, or VirlaEntry). Lentivirus was rapidly thawed at 37 °C, added to the cell suspension, gently mixed, and plated on 10 cm cell culture dishes. After 48 h, the medium was replaced with antibiotic-containing medium for selection. Selection regimes varied by antibiotic: puromycin (2.5 μg/mL, 3–4 days), blasticidin (5 μg/mL, 5–7 days), or G418 (1 mg/mL, 7–10 days). Selection continued until all negative control untransduced cells died.

To determine lentiviral titer and transduction efficiency, a serial dilution assay was performed. Cells were seeded in a 6-well plate with varying amounts of lentivirus (500 μL, 250 μL, 125 μL, 62 μL, and 32 μL) plus two control wells without lentivirus. Selection antibiotic was added to all wells except one control. This setup allowed for the determination of 100% cell survival (control without selection) and 0% transduction (control with selection). Transduction efficiency was calculated by comparing the number of surviving cells in each dilution to the 100% survival control, after subtracting the number of cells in the 0% transduction control:

$$\text{TE}_N(\%) = [(\text{NC}_N\text{-NC}_{0\%})/\text{NC}_{100\%}]/\text{Vol}_N$$

Where: TE = transduction efficiency in percentage, Vol_N = Lentivirus volume in well N, NC = number of counted cells at well N, well 0% (no virus with antibiotics selection), well 100% (no virus with no antibiotic selection). This method enabled the calculation of transduction efficiency as a percentage and the determination of functional titer in transduction units per mL.

Targeted CRISPR screening

Two CRISPR screens were conducted to identify genetic factors influencing bMSCs proliferation.

30-day screen. Cas9-expressing bMSCs were transduced with a lentiviral sgRNA library at a low multiplicity of infection (MOI ~ 0.3) to ensure approximately 600 cells per sgRNA. The screen was conducted over a 30-day period, with cells passaged every 3–4 days. DNA samples were collected at specified intervals for sgRNA quantification via next-generation sequencing (NGS). sgRNA quantification, ranking, and statistical testing were performed using MAGeCK software.

200-day screen. A second, extended CRISPR screen was performed over a 200-day timeframe. bMSCs were initially cultured for 75 days

Article

(approximately 100 doublings) before being transduced with Cas9 and the sgRNA library at a higher MOI to assess combinatorial gene knockout effects. Two control groups were included: untransduced cells and cells transduced only with Cas9. Cells were passaged and sampled as in the 30-day screen, with DNA extraction and NGS performed at specified timepoints. Data analysis was conducted using MAGeCK as in the 30-day screen. For both screens, lentiviral particles were produced as described in the "Lentivirus creation and transduction" section. Transduction efficiency was determined using the titration method outlined previously. Cell culture conditions and passaging protocols were consistent with those described in the "AD-bMSCs routine culturing" section.

DNA extraction and amplification for NGS
Genomic DNA (gDNA) was extracted from 5×10^5 cells using QuickExtract DNA Extraction Solution (Lucigen) following the manufacturer's protocol. The extracted gDNA underwent two rounds of PCR amplification. The first PCR amplified the sgRNA-containing region, and the product was purified using AMPure XP size selection beads (Beckman Coulter). The second PCR added NGS adapters to the amplicons, followed by another round of purification using two-sided size selection with AMPure XP beads. The final amplicon concentration was determined using a Qubit fluorometer, and the product size was verified on a 2% agarose gel. sgRNA amplicons were then sequenced using the xGen™ Broad-Range RNA Library Preparation Kit (IDT) on an Illumina platform at IDT/Syntezza.

RNA sequencing
Total RNA was extracted from 5×10^6 cells using TRIzol reagent (Invitrogen) followed by Direct-zol RNA Miniprep Plus Kits (Zymo Research). RNA quality was assessed using an Agilent 2200 TapeStation Bioanalyzer, and all samples had RNA Integrity Number (RIN) > 8.5. Library from total RNA was prepared using MARS-seq protocol[53], sequenced on an Illumina NovaSeq 6000 sequencer with single-end reads of 75 bp, and aligned to bovine reference genome (ARS-UCD1.2) at The Nancy and Stephen Grand Israel National Center for Personalized Medicine (G-INCPM).

CRISPR-Cas9 knockout of *PTEN* and *TP53* sgRNA design and synthesis
sgRNAs targeting *PTEN* and *TP53* were designed using the sgRNA Scorer 2.0 platform and synthesized from complementary oligonucleotides by annealing. sgRNAs were cloned into the lentiCRISPR v2 backbone plasmid using Golden Gate Assembly (Esp3I digestion). Plasmids were transformed into E. coli, selected on ampicillin plates, and verified by colony PCR. Positive clones were isolated by miniprep (Tiangen) and confirmed by Sanger sequencing. Single guide RNA sequences, as well as the primers used to construct them are found in Tables S3 and S4, respectively.

Cell culture and transfection
AD-bMSCs were seeded in 6-well plates 24 h prior to transfection. For each well, 4 μg plasmid was mixed with 400 μl Opti-MEM and 6 μl TurboFect reagent. After 20 min, the mixture was added to cells for 4 h before replacing with DMEM. Transfected cells were selected with 2.5 μg/ml puromycin for 96 h, starting 72 h post-transfection.

TP53 and PTEN KO DNA editing validation of knockout cell lines
To validate CRISPR-Cas9 editing of the target genes, genomic DNA was extracted from selected cells using QuickExtract DNA Extraction Solution (Lucigen). PCR was performed using primers flanking the targeted regions. Products were purified with SPRI beads and analyzed by agarose gel electrophoresis. The resulting amplicons were sequenced using Sanger sequencing (Hylabs, Israel). Sequencing traces were analyzed using the TIDE (Tracking of Indels by DEcomposition) bioinformatics tool to quantify editing efficiency and characterize the induced mutations. Primers for *PTEN* and *TP53* knockout validations are found in Table S5.

TP53 and PTEN KO qRT-PCR knockout validation
Cells were seeded in triplicate and cultured until they reached 80% confluency. At this point, cells were trypsinized and immediately fixed with TRI-Reagent (MRC, USA). Total RNA was then extracted using the Direct-zol RNA MiniPrep Plus kit (Zymo Research, USA), following the manufacturer's instructions. The concentration and purity of the extracted RNA were assessed using NanoDrop One spectrometer (Thermo Scientific). For cDNA synthesis, 400 ng of total RNA was reverse transcribed using the UltraScript cDNA Synthesis Kit (PCR BioSystem, USA) according to the manufacturer's protocol. Quantitative PCR (qPCR) was performed using the qPCRBIO SyGreen Blue Mix Hi-ROX (PCR BioSystem, USA) on a StepOnePlus Real-Time PCR system (Applied Biosystems). Specific primers for genes of interest and housekeeping genes are listed in Table S5. Gene expression levels were normalized to the housekeeping gene RBPs. Relative quantification of gene expression was calculated using the $2 - \Delta\Delta Ct$ method. All qPCR reactions were performed in technical triplicates for each biological replicate. Primer design and sequences can be found in Table S6.

Alamar blue cell proliferation assay
Cell proliferation was assessed using the Alamar Blue assay. Cells were seeded in 96-well plates (1000 cells/well, six replicates) and measured on days 3, 5, and 7. For each measurement, the medium was replaced with 90 μl fresh medium and 10 μl Alamar Blue reagent. After 3 h incubation at 37 °C, absorbance was measured at 540 nm.

Bioinformatic analysis
All data analysis was performed in R (v4.2.2), using tidyverse packages for general data tidying or other specialized packages for specific analysis, as detailed below. All the graphs were generated with ggplot2.

Flow cytometry
Data analysis and plot generation were performed the flowCore and ggcyto packages. Cells were gated using a two-step process: first based on forward and side scatter properties to exclude debris and doublets (FSC-A $> 3 \times 10^6$ and SSC-A $< 7.5 \times 10^6$ and exclusion of maximum FSC-A events), followed by selection of the normally distributed population using the norm2Filter function from the flowCore package. Positive expression was defined as fluorescence intensity greater than 99% of the corresponding unstained control cells. CD44 and GFP expression were analyzed using FITC fluorescence, and CD29 expression was analyzed using APC fluorescence.

CRISPR screen
CRISPR screen data analysis was conducted using custom R scripts alongside established bioinformatics tools. Raw sequencing reads were first normalized with DESeq2 to account for differences in sequencing depth across samples. sgRNA enrichment analysis was then performed using MAGeCK (Model-based Analysis of Genome-wide CRISPR-Cas9 Knockout), which applies a negative binomial model to detect significantly enriched or depleted sgRNAs between conditions. These sgRNA-level results were aggregated into gene-level scores using the robust rank aggregation (RRA) algorithm implemented in MAGeCK. To ensure data quality, we evaluated the distribution of read counts, replicate correlations, and the expected behavior of positive and negative control genes. For RNA-seq data associated with the screen, differential gene expression analysis was carried out using DESeq2. Genes were ranked based on MAGeCK scores and false discovery rates (FDR), and hits were prioritized using combined thresholds for fold change and statistical significance.

Gene ontology over-representation analysis
Gene ontology (GO) over-representation analysis was conducted to identify enriched biological processes associated with significant changes in sgRNA abundance over time. Log2 fold changes in sgRNA abundance

across multiple time points (days 0, 3, 7, 10, 16, 24, and 30) were used to cluster genes via hierarchical clustering with complete linkage based on Spearman correlation coefficients, resulting in five clusters (Fig. S3A, B). GO enrichment analysis was performed using the g:Profiler2 R package (gprofiler2), applying the gost function separately for each cluster. Genes were ranked by their maximum absolute log2 fold change values. Enriched GO terms were filtered to retain those unique to each cluster. Additional statistics calculated included term ratio, total ratio, log2 fold enrichment, and $-\log10(p$ value). To reduce redundancy among enriched terms, semantic similarity was assessed using the rrvgo package with a threshold of 0.7. The most significant term was selected as the representative for each group of similar terms.

RNA-seq
Differential expression analysis was conducted using DESeq2 in R (v4.2.2). Genes with an adjusted p value < 0.05 and |log2 fold change| > 1 were considered significantly differentially expressed. Gene Ontology (GO) enrichment analysis was performed using the clusterProfiler R package to identify significantly enriched biological processes, molecular functions, and cellular components (adjusted p value < 0.05), followed by results reduction via rrvgo R package.

Use of large language models and illustration tools
Large language models (LLMs) were employed to assist in editing and proofreading the manuscript. All LLM-generated content was subsequently reviewed and validated by the authors to ensure accuracy and prevent errors or hallucinations. Figure 1A was created using a paid, licensed BioRender account.

Statistics and reproducibility
All statistical analyses were performed in R (v4.2.2). Welch's t tests were used where appropriate. All post hoc comparisons employed Tukey's honestly significant difference (HSD) test unless otherwise noted. Effect sizes were reported as Cohen's d with 95% confidence intervals (CI). Significance thresholds were defined as follows: $p < 0.05$ (*), $p < 0.01$ (**), and $p < 0.001$ (***).

Senescence and marker expression (Fig. 1)
Senescence analysis (Fig. 1C) showed a significant effect of treatment on the percentage of senescent cells, as determined by one-way ANOVA ($F_{2,42}$ = 492.82, $p < 0.001$, η^2 = 0.96, 95% CI [0.94, 1.00]). Post hoc Tukey's HSD indicated that late-passage cells had higher senescence than early-passage cells (mean difference = 23.27, $p < 0.001$). Etoposide-treated early-passage cells showed increased senescence versus both early-passage (76.11, $p < 0.001$) and late-passage cells (52.84, $p < 0.001$).

Flow cytometry surface marker expression (Fig. 1E, n = 3 per group) showed increased CD44 in MSCs compared to control (mean difference = 1.64, 95% CI [1.59, ∞], $t(2.36)$ = 32.39, $p < 0.001$, Cohen's d = 26.44, 95% CI [7.17, ∞]) and increased CD29 (1.71, 95% CI [1.62, ∞], $t(2.14)$ = 22.79, $p < 0.001$, d = 18.61).

Lentiviral transduction efficiency (Fig. 1F) was significantly higher in MSCs (mean difference = 0.92, 95% CI [0.62, ∞], $t(2.57)$ = 7.70, p = 0.004, d = 6.44) and HEK293T cells (1.69, 95% CI [1.65, ∞], $t(2.09)$ = 143.41, $p < 0.001$, d = 117.54) relative to controls.

CRISPR screen and senescence validation (Figs. 2 and 4)
Modified hypergeometric (mHG) tests (Fig. 2C and Table S7) detected significant enrichment and depletion of sgRNAs across timepoints. TGES guides count significantly increased as early as day 3, while BGES guides count decreased by day 7 with sustained enrichment through day 30. N = 603, n_max = 603, $B_{(TGES)}$ = 73, $B_{(BGES)}$ = 46 for all days. Other parameters are found in Table S7A, B. Senescence was increased in the Cas9+Library group compared to Cas9−Library (Fig. 4C, n = 3), with a mean difference of 51.98, 95% CI [44.43, 59.53], $t(4)$ = 19.11, $p < 0.001$, d = 19.12.

qPCR and viability analyses (Fig. 6A–D)
Alamar Blue viability assays (Fig. 6A, n = 3 per group) were analyzed using a linear mixed-effects model including fixed effects for treatment and day, and a random intercept for replicate. Viability was significantly increased in *PTEN* KO (+5893, SE = 2165, $t(13)$ = 2.72, p = 0.017), *TP53* KO SC1 (+14,675, SE = 2163, $t(21)$ = 6.79, $p < 0.001$), and *TP53* KO SC2 (+17,011, SE = 2163, $t(21)$ = 7.87, $p < 0.001$). No difference was observed between SC1 and SC2 (p = 0.54).

RT-qPCR (Fig. 6D, n = 3) revealed that *TP53* expression was reduced in SC1 (mean difference = 8.62, 95% CI [7.99, 9.25], $p < 0.001$) and SC2 (9.27, 95% CI [8.64, 9.90], $p < 0.001$) vs. wild type, with SC2 slightly lower than SC1 (0.65, 95% CI [0.02, 1.28], p = 0.046). *PTEN* expression was lower in SC1 (0.97, 95% CI [0.39, 1.54], p = 0.005) and SC2 (1.34, 95% CI [0.77, 1.91], $p < 0.001$) vs. wild type, with no significant difference between SC2 and SC1 (0.38, 95% CI [−0.20, 0.95], p = 0.188).

Surface marker analysis via flow cytometry (Fig. 6B, n = 3) showed CD29 expression was elevated in P53 KO (mean difference = 1.24, 95% CI [0.76, 1.72], $t(2)$ = 11.18, p = 0.008) and *PTEN* KO (1.64, 95% CI [1.39, 1.90], $t(2)$ = 27.93, p = 0.001), but not in NC74 (0.87, 95% CI [−0.13, 1.88], $t(2)$ = 3.75, p = 0.064). CD44 was increased in NC74 (1.02, 95% CI [0.47, 1.57], $t(2)$ = 7.98, p = 0.015), P53 KO (1.36, 95% CI [0.89, 1.84], $t(2)$ = 12.34, p = 0.007), and *PTEN* KO (1.56, 95% CI [1.44, 1.66], $t(2)$ = 58.96, $p < 0.001$) relative to control.

Adipogenic differentiation (Fig. 6F, n = 3 per group) was reduced in *TP53* KO SC1 (mean difference = 40.35%, SE = 5.38, $t(10)$ = 7.50, $p < 0.001$) and SC2 (19.96%, $t(10)$ = 3.71, p = 0.026), as well as *PTEN* KO SC1 (57.67%, $t(10)$ = 10.73, $p < 0.001$) and SC2 (27.00%, $t(10)$ = 5.02, p = 0.0037), compared to wild type.

Data availability
Next-generation sequencing (NGS) source data from this study have been deposited in the Gene Expression Omnibus (GEO) and can be obtained under the following accession numbers: GSE280666 (Long-term 100-day CRISPR screen), GSE280675 (RNA sequencing data), GSE280676 (Short-term 30-day CRISPR screen). Flow cytometry source data from this study have been deposited in figshare and can be obtained as follows[54–56]. CD44 and CD29 Expression in Naïve bMSCs—Flow Cytometry Data (Fig. 1E). figshare. Dataset. https://figshare.com/s/700074fe372ae24101d1. GFP Expression in Lentivirus-Transduced bMSCs—Flow Cytometry Data (Fig. 1F). figshare. Dataset. https://figshare.com/s/700074fe372ae24101d1. CD44 and CD29 Expression in *TP53* and *PTEN* KO bMSCs—Flow Cytometry Data (Fig. 6B). figshare. Dataset. https://figshare.com/s/9985941bc68e66a0d6f6. All other relevant source data is provided in the Supplementary Materials file ("Supplementary Data.xlsx"). Any other data supporting the findings of this study are available from the corresponding author upon reasonable request. Unedited and uncropped gel of Fig. 1G is provided in Supplementary Fig. S2F.

Code availability
All analyses were performed using standard packages and publicly available software, as detailed in the "Methods" section. The custom code used for data analysis in this study is available from the corresponding author upon reasonable request.

References
1. FAOSTAT: Crops and livestock products. FAO (2025).
2. OECD/FAO. *OECD-FAO Agricultural Outlook 2021–2030* (OECD Publishing, 2021).
3. World Bank. *Population, Total*. UN Statistics Division (2025).
4. Godfray, H. C. J. et al. Meat consumption, health, and the environment. *Science* **361**, eaam5324 (2018).

5. Fuhlendorf, S. D. & Engle, D. M. Restoring heterogeneity on rangelands: ecosystem management based on evolutionary grazing patterns: we propose a paradigm that enhances heterogeneity instead of homogeneity to promote biological diversity and wildlife habitat on rangelands grazed by livestock. *BioScience* **51**, 625–632 (2001).

6. Hoekstra, A. Y. & Mekonnen, M. M. The water footprint of humanity. *Proc. Natl. Acad. Sci. USA* **109**, 3232–3237 (2012).

7. Beal, T. et al. Friend or foe? The role of animal-source foods in healthy and environmentally sustainable diets. *J. Nutr.* **153**, 409–425 (2023).

8. Van Boeckel, T. P. et al. Global trends in antimicrobial use in food animals. *Proc. Natl. Acad. Sci. USA* **112**, 5649–5654 (2015).

9. Post, M. J. Cultured meat from stem cells: challenges and prospects. *Meat Sci*. **92**, 297–301 (2012).

10. Ben-Arye, T. & Levenberg, S. Tissue engineering for clean meat production. *Front. Sustain. Food Syst*. **3**, 46 (2019).

11. Dodson, M. V. et al. INVITED REVIEW: Evolution of meat animal growth research during the past 50 years: adipose and muscle stem cells. *J. Anim. Sci.* **93**, 457–481 (2015).

12. Bacakova, L. et al. Stem cells: their source, potency and use in regenerative therapies with focus on adipose-derived stem cells — a review. *Biotechnol. Adv.* **36**, 1111–1126 (2018).

13. Foley, J. A. et al. Solutions for a cultivated planet. *Nature* **478**, 337–342 (2011).

14. O'Neill, E. N., Cosenza, Z. A., Baar, K. & Block, D. E. Considerations for the development of cost-effective cell culture media for cultivated meat production. *Compr. Rev. Food Sci. Food Saf.* **20**, 686–709 (2021).

15. Post, M. J. et al. Scientific, sustainability and regulatory challenges of cultured meat. *Nat. Food* **1**, 403–415 (2020).

16. Hauser, M., Zirman, A., Rak, R. & Nachman, I. Challenges and opportunities in cell expansion for cultivated meat. *Front. Nutr*. **11**, 1315555 (2024).

17. Reiss, J., Robertson, S. & Suzuki, M. Cell sources for cultivated meat: applications and considerations throughout the production workflow. *Int. J. Mol. Sci.* **22**, 7513 (2021).

18. The Good Food Institute. Cultivated meat media and growth factor trends: cell lines and types. https://gfi.org/resource/cultivated-meat-media-growth-factor-survey/#cell-lines-and-types (2024).

19. Pittenger, M. F. et al. Multilineage potential of adult human mesenchymal stem cells. *Science* **284**, 143–147 (1999).

20. LH, O. et al. Myogenic differentiation potential of mesenchymal stem cells derived from fetal bovine bone marrow. *Anim. Biotechnol.* **29**, 1–11 (2018).

21. Heyman, E. et al. Evaluation of enzymatic protocols to optimize efficiency of bovine adipose tissue-derived mesenchymal stromal cell isolation. *Npj Sci. Food* **8**, 70 (2024).

22. Zomer, H. D., Vidane, A. S., Gonçalves, N. N. & Ambrósio, C. E. Mesenchymal and induced pluripotent stem cells: general insights and clinical perspectives. *Stem Cells Cloning Adv. Appl.* **8**, 125–134 (2015).

23. Lin, J. & Epel, E. Stress and telomere shortening: Insights from cellular mechanisms. *Ageing Res. Rev.* **73**, 101507 (2022).

24. Weng, Z. et al. Mesenchymal stem/stromal cell senescence: hallmarks, mechanisms, and combating strategies. *Stem Cells Transl. Med.* **11**, 356–371 (2022).

25. Shalem, O., Sanjana, N. E. & Zhang, F. High-throughput functional genomics using CRISPR-Cas9. *Nat. Rev. Genet.* **16**, 299–311 (2015).

26. Joung, J. et al. Genome-scale CRISPR-Cas9 knockout and transcriptional activation screening. *Nat. Protoc.* **12**, 828–863 (2017).

27. Sampaio, R. V. et al. Generation of bovine (Bos indicus) and buffalo (Bubalus bubalis) adipose tissue derived stem cells: isolation, characterization, and multipotentiality. *Genet Mol. Res.* **14**, 53–62 (2015).

28. de Souza, M. M. et al. A comprehensive manually-curated compendium of bovine transcription factors. *Sci. Rep.* **8**, 13747 (2018).

29. DepMap, B. DepMap 23Q4 Public. https://doi.org/10.25452/figshare.plus.24667905.v2 (2023).

30. Tan, W. S. et al. GARP and EARP are required for efficient BoHV-1 replication as identified by a genome wide CRISPR knockout screen. *PLoS Pathog*. **19**, e1011822 (2023).

31. Li, W. et al. MAGeCK enables robust identification of essential genes from genome-scale CRISPR/Cas9 knockout screens. *Genome Biol.* **15**, 554 (2014).

32. Eden, E., Lipson, D., Yogev, S. & Yakhini, Z. Discovering motifs in ranked lists of DNA sequences. *PLoS Comput. Biol.* **3**, e39 (2007).

33. Hernández Borrero, L. J. & El-Deiry, W. S. Tumor suppressor p53: biology, signaling pathways, and therapeutic targeting. *Biochim. Biophys. Acta* **1876**, 188556 (2021).

34. Jung, S. H. et al. mTOR kinase leads to *PTEN*-loss-induced cellular senescence by phosphorylating p53. *Oncogene* **38**, 1639–1650 (2019).

35. Kolberg, L., Raudvere, U., Kuzmin, I., Vilo, J. & Peterson, H. gprofiler2 — an R package for gene list functional enrichment analysis and namespace conversion toolset g:Profiler. *F1000Research* **9**, ELIXIR-709 (2020).

36. Oughtred, R. et al. The BioGRID database: a comprehensive biomedical resource of curated protein, genetic, and chemical interactions. *Protein Sci. Publ. Protein Soc.* **30**, 187–200 (2021).

37. Lee, Y.-R., Chen, M. & Pandolfi, P. P. The functions and regulation of the *PTEN* tumour suppressor: new modes and prospects. *Nat. Rev. Mol. Cell Biol.* **19**, 547–562 (2018).

38. Ruijtenberg, S. & van den Heuvel, S. Coordinating cell proliferation and differentiation: antagonism between cell cycle regulators and cell type-specific gene expression. *Cell Cycle* **15**, 196–212 (2016).

39. Molchadsky, A. et al. p53 plays a role in mesenchymal differentiation programs, in a cell fate dependent manner. *PLoS ONE* **3**, e3707 (2008).

40. Armesilla-Diaz, A., Elvira, G. & Silva, A. p53 regulates the proliferation, differentiation and spontaneous transformation of mesenchymal stem cells. *Exp. Cell Res.* **315**, 3598–3610 (2009).

41. Hallenborg, P., Feddersen, S., Madsen, L. & Kristiansen, K. The tumor suppressors pRB and p53 as regulators of adipocyte differentiation and function. *Expert Opin. Ther. Targets* **13**, 235–246 (2009).

42. Tavoulari, S., Sichrovsky, M. & Kunji, E. R. S. Fifty years of the mitochondrial pyruvate carrier: new insights into its structure, function, and inhibition. *Acta Physiol* **238**, e14016 (2023).

43. Farook, M. R. et al. Loss of mitochondrial pyruvate carrier 1 supports proline-dependent proliferation and collagen biosynthesis in ovarian cancer. *Mol. Metab.* **81**, 101900 (2024).

44. Liberti, M. V. & Locasale, J. W. The Warburg effect: how does it benefit cancer cells? *Trends Biochem. Sci.* **41**, 211–218 (2016).

45. Li, Q., Gao, Z., Chen, Y. & Guan, M.-X. The role of mitochondria in osteogenic, adipogenic and chondrogenic differentiation of mesenchymal stem cells. *Protein Cell* **8**, 439–445 (2017).

46. Mandal, S., Lindgren, A. G., Srivastava, A. S., Clark, A. T. & Banerjee, U. Mitochondrial function controls proliferation and early differentiation potential of embryonic stem cells. *Stem Cells* **29**, 486–495 (2011).

47. Baas, R. et al. Quantitative proteomics of the SMAD (Suppressor of Mothers against Decapentaplegic) transcription factor family identifies importin 5 as a bone morphogenic protein receptor SMAD-specific importin *. *J. Biol. Chem.* **291**, 24121–24132 (2016).

48. LeBlanc, K. T. et al. Runx1 activities in superficial zone chondrocytes, osteoarthritic chondrocyte clones and response to mechanical loading. *J. Cell. Physiol.* **230**, 440–448 (2015).

49. Wilkinson, D. J. Serpins in cartilage and osteoarthritis: what do we know? *Biochem. Soc. Trans.* **49**, 1013–1026 (2021).

50. Riquelme-Guzmán, C., Stout, A. J., Kaplan, D. L. & Flack, J. E. Unlocking the potential of cultivated meat through cell line engineering. *iScience* **27**, 110877 (2024).
51. Jaime-Rodríguez, M., Cadena-Hernández, A. L., Rosales-Valencia, L. D., Padilla-Sánchez, J. M. & Chavez-Santoscoy, R. A. Are genetic drift and stem cell adherence in laboratory culture issues for cultivated meat production? *Front. Nutr.* **10**, 1189664 (2023).
52. Doxzen, K. & Henderson, H. Is this safe? Addressing societal concerns about CRISPR-edited foods without reinforcing GMO framing. *Environ. Commun.* **14**, 865–871 (2020).
53. Keren-Shaul, H. et al. MARS-seq2.0: an experimental and analytical pipeline for indexed sorting combined with single-cell RNA sequencing. *Nat. Protoc.* **14**, 1841–1862 (2019).
54. Zirman, A. et al. CD44 and CD29 Expression in Naïve bMSCs – Flow Cytometry Data (Fig 1E). figshare dataset. https://figshare.com/articles/dataset/CD44_and_CD29_Expression_in_Na_ve_bMSCs_Flow_Cytometry_Data_Fig_1E_/29381993 (2025).
55. Zirman, A. et al. CD44 and CD29 Expression in TP53 and PTEN KO bMSCs – Flow Cytometry Data (Fig 6B). figshare dataset. https://figshare.com/articles/dataset/CD44_and_CD29_Expression_in_TP53_and_PTEN_KO_bMSCs_Flow_Cytometry_Data_Fig_6B_/29390804 (2025).
56. Zirman, A., et al. GFP Expression in Lentivirus-Transduced bMSCs – Flow Cytometry Data (Fig 1F). figshare dataset. https://figshare.com/articles/dataset/GFP_Expression_in_Lentivirus-Transduced_bMSCs_Flow_Cytometry_Data_Fig_1F_/29382107 (2025).

Author contributions

A.Z. designed and performed experiments, analyzed data, and wrote the manuscript. M.A.N. isolated and characterized AD-bMSCs. E.S. performed single-gene knockout validations of *PTEN* and *TP53*. Z.Y. contributed to bioinformatics design, analysis, and manuscript review. L.A. contributed to bioinformatics design, analysis, and manuscript review. I.N. supervised the project, contributed to experimental design, and reviewed the manuscript. R.R. conceived and supervised the project, designed experiments, provided tools and materials, analyzed data, and critically revised the manuscript.

Competing interests

The authors declare no competing interests.

Ethical approval

All procedures involving animals were approved by the Animal Experimentation Ethics Committee of the Volcani Center, Agricultural Research Organization, Ministry of Agriculture and Rural Development, Israel (approval numbers IL970/23 and VOL-IL-2301-103-3). The committee was chaired by Dr. Maya Ross. We have complied with all relevant ethical regulations for animal use. The study involved the isolation of stem cells from a live female calf (*Bos taurus*, approximately 3 months old), conducted under approved conditions at the Volcani Institute dairy farm.

Additional information

Supplementary information The online version contains supplementary material available at https://doi.org/10.1038/s42003-025-08760-y.

Correspondence and requests for materials should be addressed to Roni Rak.

Peer review information *Communications Biology* thanks Joshua Flack and the other, anonymous, reviewer(s) for their contribution to the peer review of this work. Primary Handling Editors: Dr Ophelia Bu and Dr Mengtan Xing.

Reprints and permissions information is available at http://www.nature.com/reprints

Publisher's note Springer Nature remains neutral with regard to jurisdictional claims in published maps and institutional affiliations.